Supporting Information (SI)

Engineering hollow carbon spheres: Directly from solid resin spheres to porous hollow carbon spheres via air induced linker cleaving

Neng Li[a], Bihui Qin[a], Hongfei Kang[a], Nana Cai[a], Suping Huang[b], Qi Xiao[a]*

a School of Minerals Processing and Bioengineering, Central South University, Changsha 410083, China.

b State Key Lab of Powder Metallurgy, Central South University, Changsha 410083, China.

*Corresponding author: Qi Xiao

E-mail: xiaoqi88@csu.edu.cn.

Tel: +86-731-88830543. Fax: +86-731-88879815.

Section 1

1.1. Materials Characterization

The XRD patterns of the sample was recorded with a DX-2700 X-ray powder diffractometer (XRD) with Cu Kα radiation ($\lambda = 1.54056$Å). The morphologies of the samples were characterized with scanning electronic microscopy (SEM, ZEISS Signa 300) and transmission electron microscope (TEM, FEI Tecnai G2 f20 s-twin 299Kv). The X-ray photoelectron spectra (XPS) measurements were performed on a VG Scientific ESCA-LAB Mark Ⅱ spectrometer equipped with two ultrahigh vacuum (UHV) chambers using Al Kα radiation (1486.6 eV) to investigate the surface properties. The binding energy of the XPS spectra is calibrated with the reference to the C 1s peak (284.8 eV) arising from adventitious carbon. The nitrogen adsorption and desorption isotherms were collected at 77 K on a Micromeritic ASAP 2460 instrument. The specific surface areas were calculated using the Brunnauer-Emmett-Teller (BET) equation and the pore size distributions were calculated by applying the Barrett-Joyner-Halenda (BJH) method using the desorption branch of the isotherms. The Fourier transform infrared (FTIR) spectroscopy analysis was conducted on a Nicolet iS50 FTIR spectrometer. The Raman spectrum analysis was conducted on a Labram HR800 Laser Raman Spectroscopy made by Jobin Yvon, France, using the 632.8 nm He-Ne ion laser as an excitation source. The laser power on the sample was 10 mW.

1.2. Electrochemical Measurement

Lithium metal was used as the anode electrode. The electrolyte composition contains 1M lithium bistrifluoromethanesulfonylimide (LITFSI) and 0.1 M lithium nitrate (LiNO3) salts dissolved in a mixed solvent of 1,2-dimethoxyethane (DME) and 1,3-dioxolane (DOL) (volume ratio 1:1). The electrochemical measurements were performed with 2025 coin-type cells. The cells were assembled in an Ar-filled glovebox with moisture and oxygen concentrations below 0.1 ppm.

The charge/discharge measurements were conducted on Neware BTS4000 battery test system (Shenzhen, Chain) in a voltage range between 1.7 V and 2.8 V. Cyclic voltammetry (CV) measurements were measured by using the Gamry Interface 1000T electrochemical workstation at different scan rates in the voltage range of 1.7-2.8 V versus Li/Li^+, and the electrochemical impedance spectroscopy(EIS) measurements were performed on the same of electrochemical workstation by applying a sine wave with amplitude of 5.0mV over the frequency range from 100KHz to 0.1Hz.

Section 2

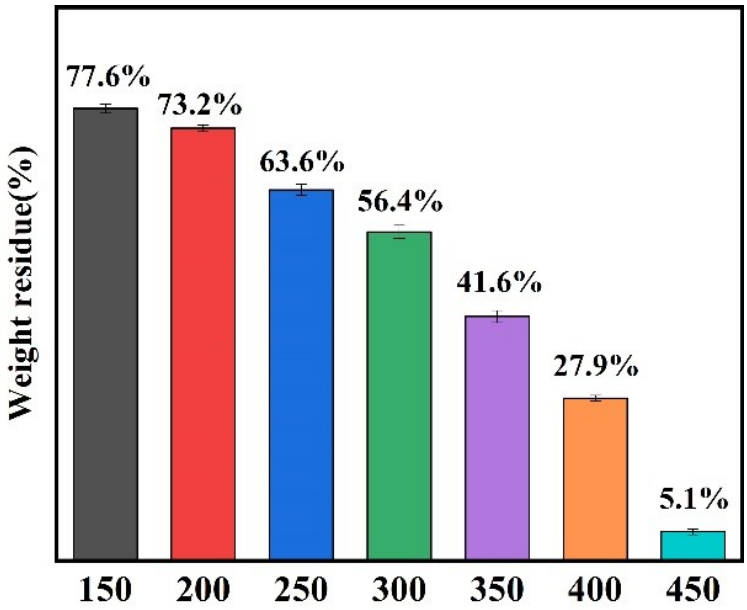

Fig.S1. The weight residue of APF spheres calcined at different temperatures in air.

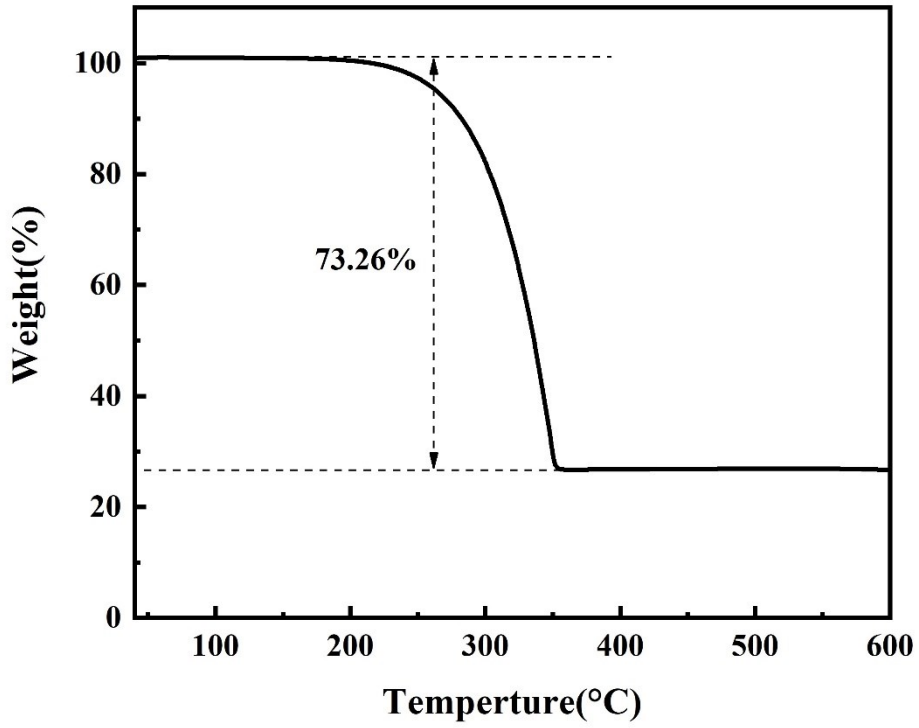

Fig. S2. TG curve of the Super P/S composites under N_2 atmosphere with a heating rate of 5℃/min.

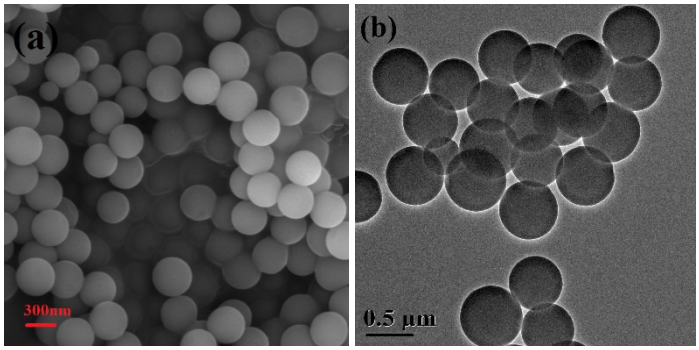

Fig. S3. (a) SEM, and (b) TEM images of solid APF spheres.

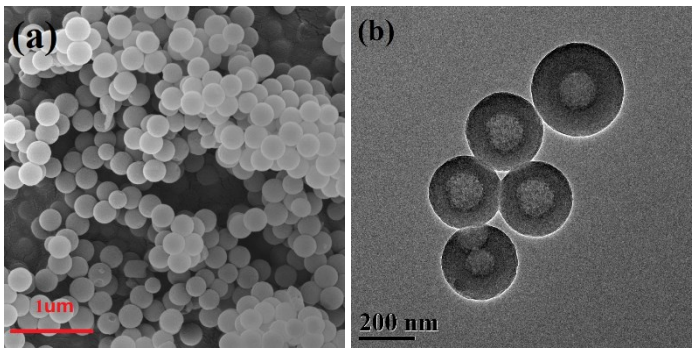

Fig. S4. (a) SEM, and (b) TEM images of HCS/400 spheres.

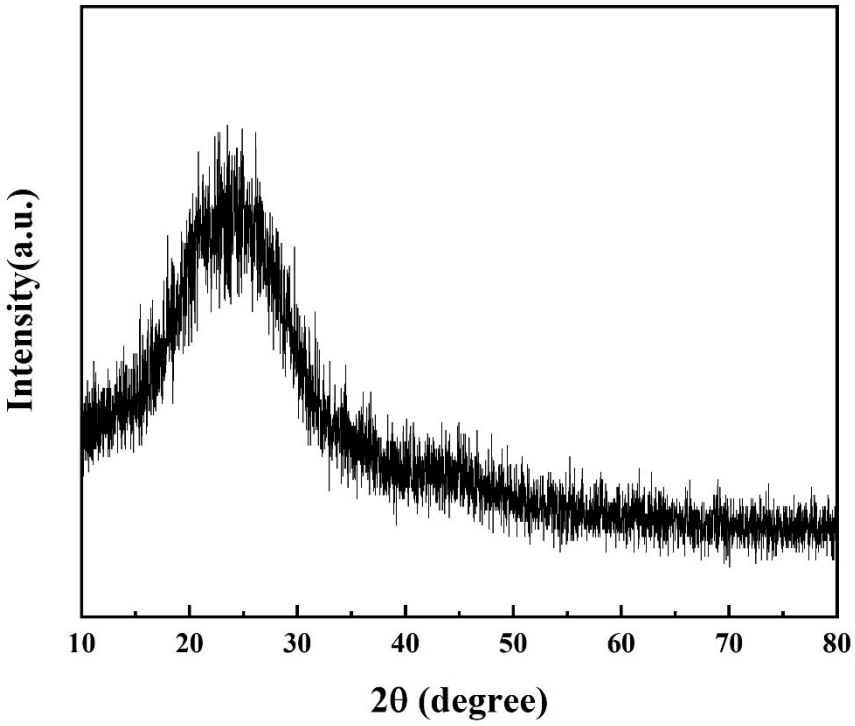

Fig. S5. XRD pattern of HCS/400.

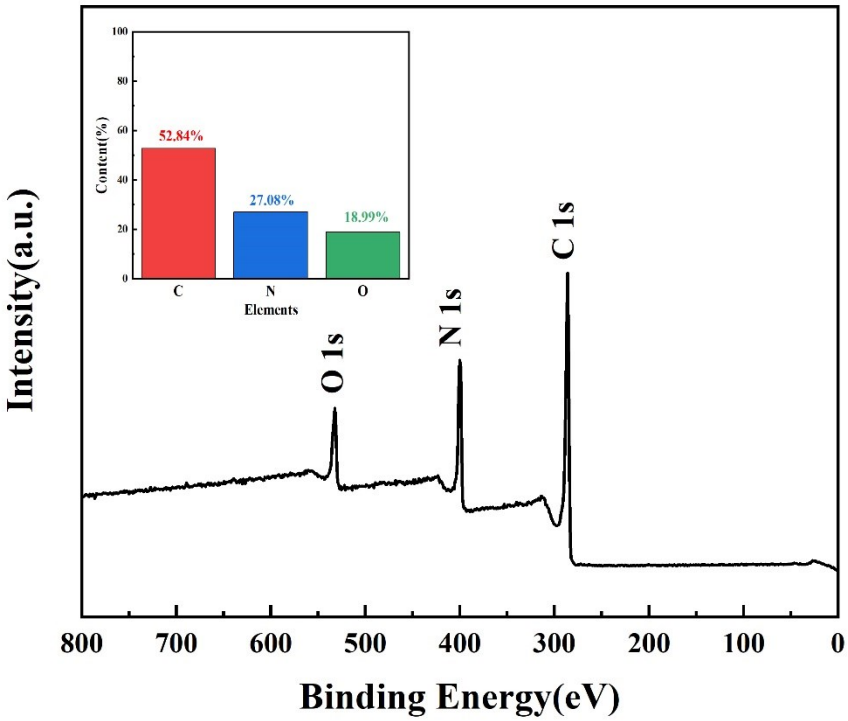

Fig. S6: XPS pattern of HCS/400.

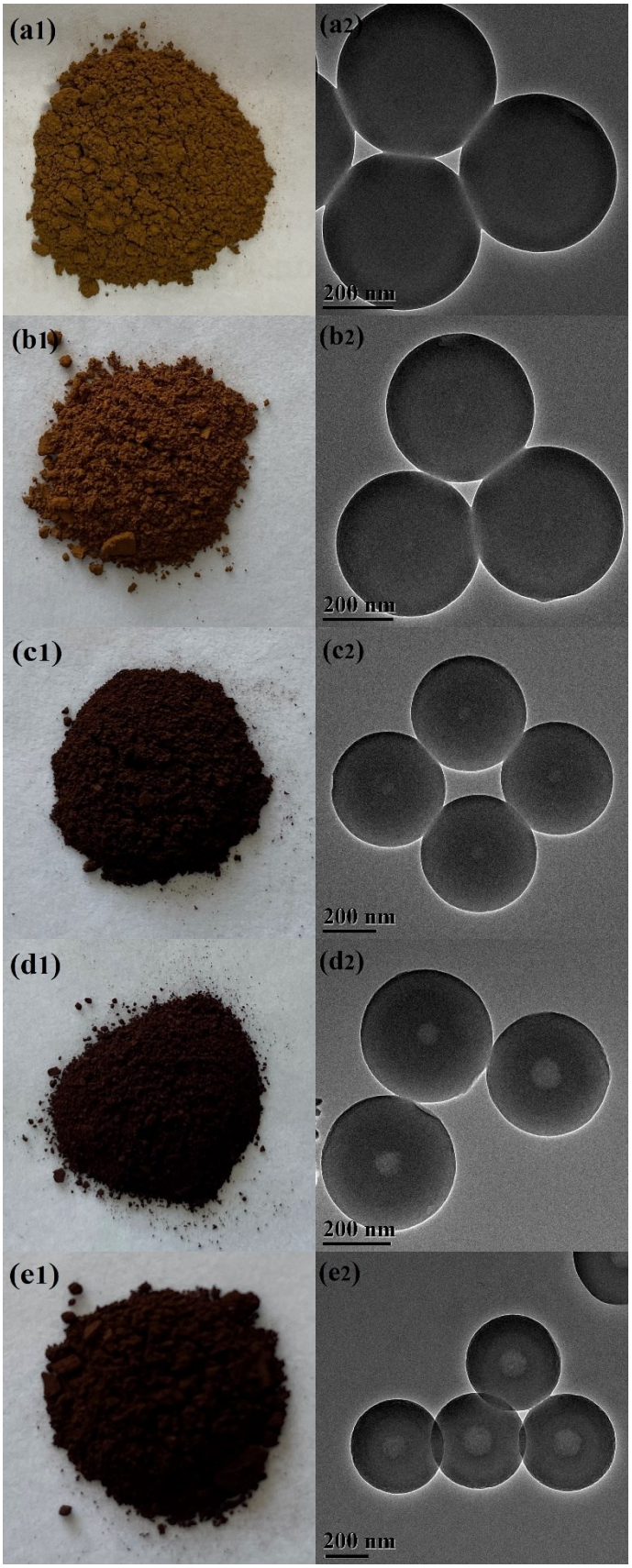

Fig. S7: Photograph and TEM images of APF spheres at different oxidative linker cleaving temperature under air atmosphere: a) 150°C, b) 200°C, c) 250°C, d) 300°C, e) 350°C.

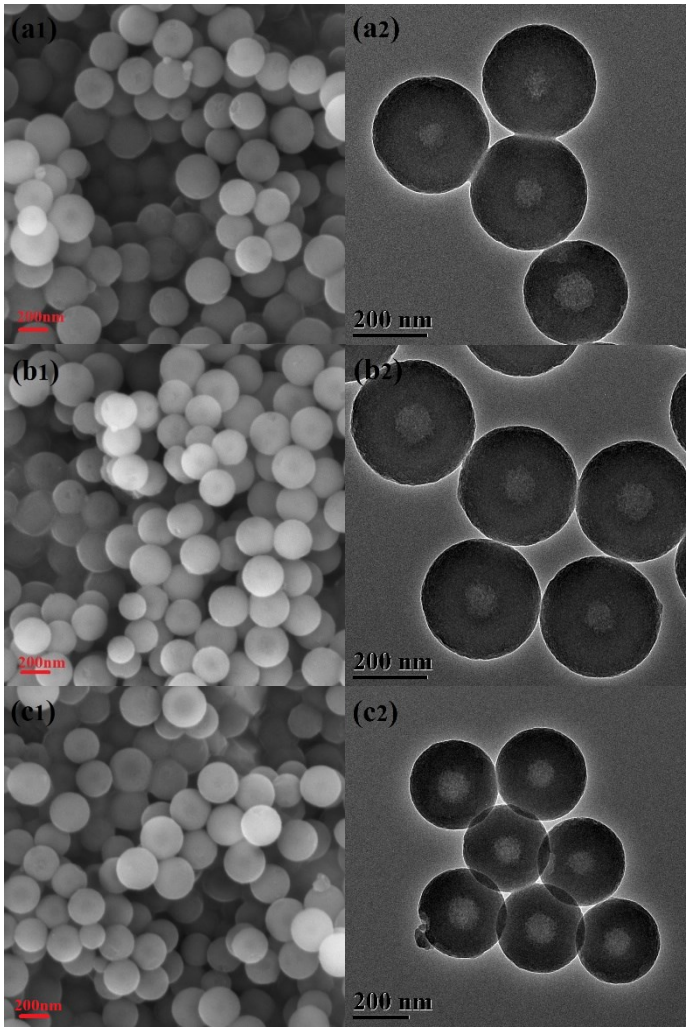

Fig. S8. SEM and TEM images of APF spheres at different oxidative linker cleaving time under air atmosphere at 400°C: a) 10min, b) 20min, c) 40min.

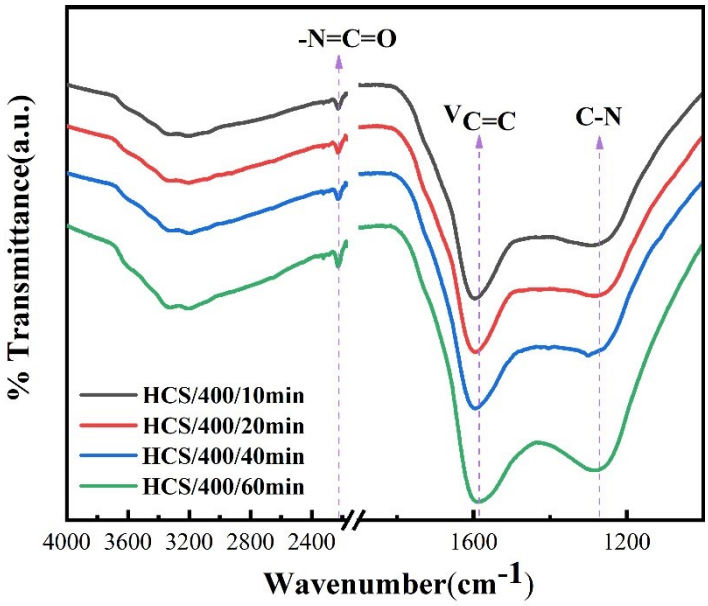

Fig. S9. The Fourier transform infrared (FTIR) spectrum of solid APF spheres synthesized at different oxidative linker cleaving time under air atmosphere at 400°C.

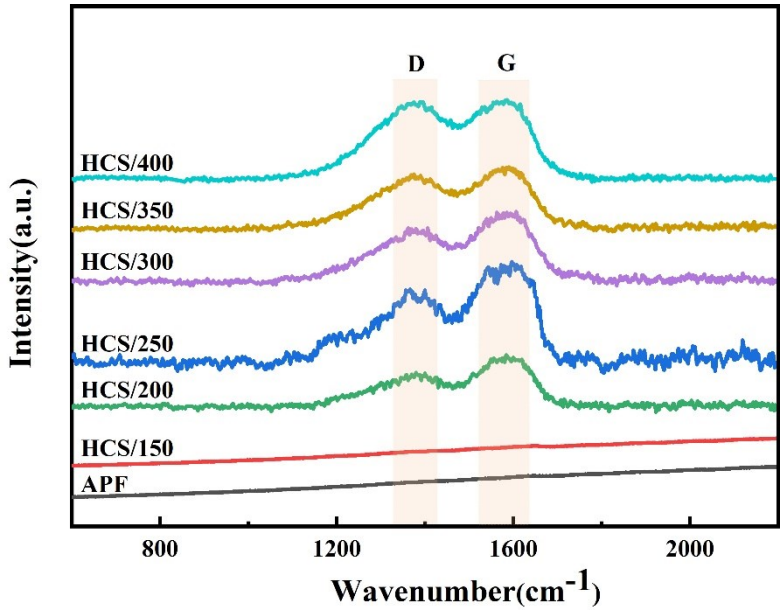

Fig. S10. The Raman diagram of solid APF spheres synthesized at different oxidative linker cleaving temperature under air atmosphere.

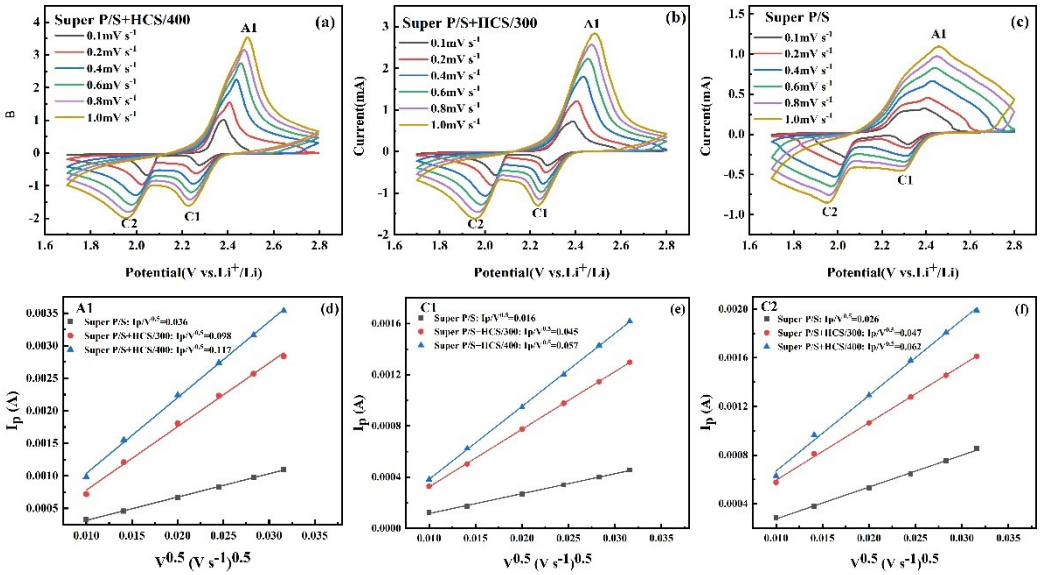

Fig.S11: CV curves of LSBs with a) Super P/S+HCS/400, b) Super P/S+HCS/300, and c) Super P/S at different scan rate. Points and fitted lines of CV peak current versus square root scan rates for d) A1, e) C1, and f) C2 peaks.

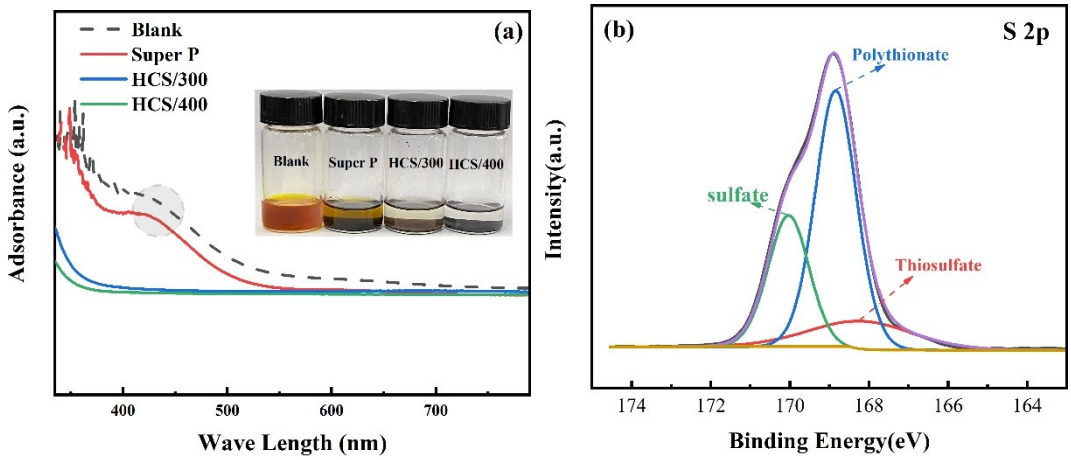

Fig.S12. (a) UV-vis spectra of Li_2S_n solutions with DOL/DME solvents (1:1, v/v) and those after adsorption by conductive acetylene black (Super P), HCS/300 and HCS/400, insets: photographs of blank solution and the solutions after adding conductive acetylene black (Super P), HCS/300 and HCS/400. (b) XPS spectra of S 2p for Li_2S_n solutions after adsorption by HCS/400.

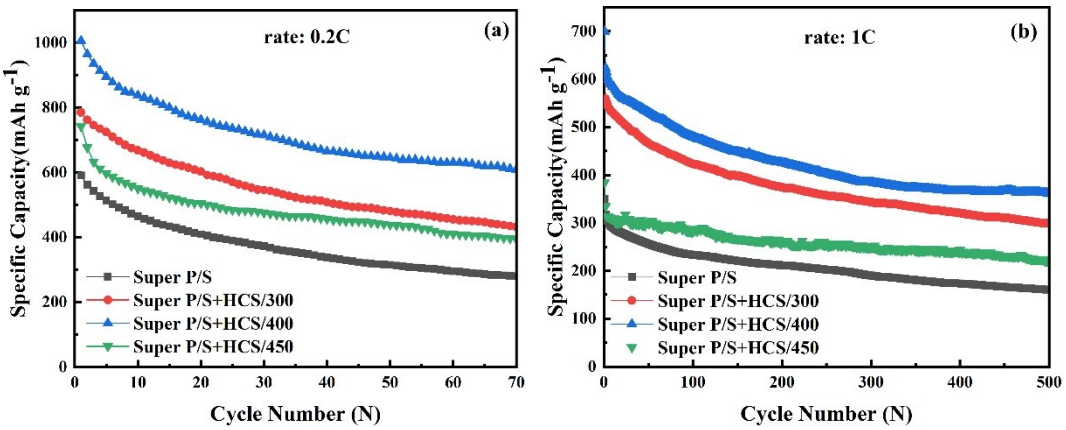

Fig.S13. (a) Cycling performances of at 0.2 C for 70 cycles; (b) Cycling performances and Columbic efficiency at 1C for 500 cycles of Super P/S, Super P/S+HCS/300, Super P/S+HCS/400, Super P/S+HCS/450 cathode.

Table S1. HCSs outer diameter, shell thickness and hollow size of oxidative linker cleaving at different temperatures in air atmosphere.

Samples	Outer Diameters (nm)	Shell Thickness (nm)	Hollow Size (nm)
APF	~600	~300	0
HCS/150	~444	~222.22	0
HCS/200	~438	~209	~20
HCS/250	~414	~178	~57
HCS/300	~400	~162	~76
HCS/350	~340	~107	~126
HCS/400	~325	~77	~171

Table S2. HCSs outer diameter, shell thickness and hollow size of oxidative linker cleaving at different time for 400℃ under air atmosphere

Time	Outer Diameters /nm	Shell Thickness /nm	Hollow Size /nm
10min	360	130	100
20min	340	120	100
40min	330	103	124

Table S3: The change of chemical functional groups of APF and HCS at different thermal treatment temperature in air (Strong, Weak, and No).

Wavenumber (cm^{-1})	Chemical functional group	APF	HCS/ 150	HCS/ 200	HCS/ 250	HCS/ 300	HCS/ 350	HCS/ 400
~2934 ~2853	$-CH_2-$	**S**	**W**	**N**	**N**	**N**	**N**	**N**
~2226	-N=C=O	**N**	**N**	**N**	**W**	**W**	**S**	**S**
~1621 ~1451	C=C stretching for phenol ring	**S**	**S**	**S**	**S**	**S**	**S**	**S**
~1283	C-N	**S**	**S**	**S**	**S**	**S**	**S**	**S**
~1239	Ar-O-C	**S**	**W**	**N**	**N**	**N**	**N**	**N**
~1186 ~1117	C-O-C	**S**	**N**	**N**	**N**	**N**	**N**	**N**

Table S4: The integral intensity values of D and G peaks of the obtained samples measured from Raman results.

Samples	**I_D**	**I_G**	**I_D/I_G**
HCS/200	120034.7	247953.2	0.484
HCS/250	76603.1	140312.4	0.546
HCS/300	95652.8	131519.1	0.727
HCS/350	79253.4	104683.3	0.757
HCS/400	57692.3	65669.6	0.878

Table S5. The redox peaks of the three cathode materials with the corresponding D_{Li^+}.

S Cathode	D_{Li^+} of A1 peak ($cm^2 S^{-1}$)	D_{Li^+} of C1 peak ($cm^2 S^{-1}$)	D_{Li^+} of C2 peak ($cm^2 S^{-1}$)
Super P/S+HCS/400	8.24×10^{-9}	1.96×10^{-9}	2.31×10^{-9}
Super P/S+HCS/300	5.78×10^{-9}	1.22×10^{-9}	1.33×10^{-9}
Super P/S	7.8×10^{-10}	1.54×10^{-10}	4.07×10^{-10}

Table. S6. The comparisons of cyclic performance of Super P/S+HCS/400 cathode with other materials reported in the previous works

Host material	cathode	sulfur Content (wt%)	C-rate	Cycle number	Initial capacity (mAh g^{-1})	Reversible capacity (mAh g^{-1})	Ref.
conductive acetylene black	Super P/S +HCS/400	51.3%	0.2C	70	1006	647.8	This paper
N doped hollow carbon spheres	S/N-HCS	49%	0.2C	50	1072	750.4	[1]
Functionalized N doped hollow carbon spheres	F-NHCS-S	59.2%	0.2C	100	827	549	[2]
N-doped hollow carbon nanospheres	NMHC-2-S	65.4%	0.2C	100	1113	800	[3]

References:

[1] Pei F, An T, Zang J, et al. From Hollow Carbon Spheres to N-Doped Hollow Porous Carbon Bowls: Rational Design of Hollow Carbon Host for Li-S Batteries[J]. Advanced Energy Materials, 2016, 6(8).

[2] Li X, Pan Z, Li Z, et al. Functionalized N-doped hollow carbon spheres as sulfur host with enhanced electrochemical performances of lithium-sulfur batteries[J]. Ionics, 2019, 25(2): 503-511.

[3] Zhou W, Wang C, Zhang Q, et al. Tailoring Pore Size of Nitrogen-Doped Hollow Carbon Nanospheres for Confining Sulfur in Lithium-Sulfur Batteries[J]. Advanced Energy Materials, 2015, 5(16).